



Hybrid Optimization Algorithm Enabled Deep Learning Approach Brain Tumor Segmentation and Classification Using MRI

S. Deepa¹ · J. Janet² · S. Sumathi³ · J. P. Ananth²

Received: 4 July 2022 / Revised: 16 September 2022 / Accepted: 4 December 2022 / Published online: 9 January 2023
© The Author(s) under exclusive licence to Society for Imaging Informatics in Medicine 2023

Abstract

The unnatural and uncontrolled increase of brain cells is called brain tumors, leading to human health danger. Magnetic resonance imaging (MRI) is widely applied for classifying and detecting brain tumors, due to its better resolution. In general, medical specialists require more details regarding the size, type, and changes in small lesions for effective classification. The timely and exact diagnosis plays a major role in the efficient treatment of patients. Therefore, in this research, an efficient hybrid optimization algorithm is implemented for brain tumor segmentation and classification. The convolutional neural network (CNN) features are extracted to perform a better classification. The classification is performed by considering the extracted features as the input of the deep residual network (DRN), in which the training is performed using the proposed chronological Jaya honey badger algorithm (CJHBA). The proposed CJHBA is the integration of the Jaya algorithm, honey badger algorithm (HBA), and chronological concept. The performance is evaluated using the BRATS 2018 and Figshare datasets, in which the maximum accuracy, sensitivity, and specificity are attained using the BRATS dataset with values 0.9210, 0.9313, and 0.9284, respectively.

Keywords Normalization · Gaussian noise · Chronological concept · Honey badger algorithm · Data augmentation

Introduction

The human body's complex and massive organ is the brain, which consists of almost 100 billion nerve cells. It presents in the middle of the nervous system, which controls all the nervous systems [1]. Hence, the abnormalities in the brain lead to danger to human health. In such abnormalities, the most dangerous one is the brain tumor, which is defined as the unnatural and uncontrolled increase of cells in the brain. Primary and secondary tumors are the two categories of brain tumors. The availability of tumors in the brain tissue is called primary tumors. When the other human body parts, tumor cells, are moved to brain tissue through the blood-stream and form tumors, it is called secondary tumors [2, 3].

The symptoms of brain tumors vary due to the location and type of the tumors, and some of the symptoms are unusual behavior, memory issues, seizures, changes in vision, balance issues, and confusion [4]. To treat, monitor, diagnose, and analyze the human body, various medical imaging approaches are successfully used, which are X-rays, ultrasound imaging (UI), computerized tomography (CT), and MRI. Among these imaging technologies, the MRI is widely used for classifying and detecting due to its better resolution [5] and is also commonly used for identifying brain tumors. The reason for using MRI in identifying tumors is during the MRI scan, non-ionizing radiation is produced, which is able to acquire various images by applying numerous image parameters [6, 7]. The tumor diagnosis has four MRI modalities, and the images are produced with various tissue variations in every modality. Hence, MRI is more suitable than other techniques for segmenting and classifying the tumors in the brain [6].

The exact brain tumor segmentation and classification lead to offering better treatment [8]. The main motive of segmenting a tumor is to separate the tumor brain tissues, like necrotic core, edema, and active cells, from the regular brain tissues, like cerebrospinal fluid (CSF), gray matter

✉ S. Deepa
dineshdeepas1977@gmail.com

¹ Professor, Department of ECE, Panimalar Engineering College, Chennai, India

² Professor, Department of CSE, Sri Krishna College of Engineering and Technology, Coimbatore, India

³ Professor, Department of EEE, Mahendra Engineering College, Namakkal, India

(GM). Recently, the segmentation approaches have been categorized on the basis of numerous principles, and the three major categories in segmentation are fully automatic, semi-automatic, and manual segmentations [9, 10]. The classification of tumors in the brain helps doctors to attain an exact diagnosis that plays a major role in the efficient treatment for patients [11]. The manual and automatic classifications are the two types of brain tumor classification, in which the manual process is a challenging and tricky task. In the manual process, the classification of MRIs with the same appearances and structures are required the radiologist's expertise available for identifying and classifying the tumors [12]. In the past years, various techniques have been developed for effective classification with the help of high-resolution MRI images of the brain with sensible contrast [5].

The advancement of machine learning and artificial intelligence techniques are offering a better impact on the medical area and are significant support tools in medical departments. For supporting the decisions of radiologist, numerous automatic learning schemes are applied for the segmentation and classification [34–36]. However, because of high intra and inter-shape, contrast variations, and texture, the classification is difficult in the traditional approaches [2, 32, 33]. The supervised techniques need expertise for extracting the best features and technique selection for the classification of brain tumors [13, 14]. Recently, unsupervised techniques [15] have been used by many researchers because of better performance, automatic feature generation, and minimized error rate. Also, deep learning (DL)-based techniques are essential in healthcare image analysis, like segmentation [16], reconstruction [17], and classification [18]. Moreover, these DL techniques are used in the automatic extraction of meaningful features for obtaining better results.

Accordingly, an efficient optimization-enabled deep learning technique is developed in this research for segmenting and classifying brain tumors. Here, MRI is the input, which is passed to the pre-processing phase for enhancing the image quality by removing the noises using normalization. Then, the DeepMRSeg [19] is used in the segmentation, which is training using CHBA. The CHBA is the integration of HBA [20] and chronological concept. After segmenting, the CNN features [21] are extracted for proceeding the next step. Then, the data augmentation is achieved by means of randomized left or right flipping, rotation and brightness or contrast adjustment, random translation, and including Gaussian noise. After augmenting data, the classification is performed using DRN [22], in which the training is performed using the proposed CJHBA. The proposed CJHBA is the integration of the Jaya algorithm [23], HBA, and chronological concept.

The contributions of this research:

- Proposed CHBA-Based DeepMRSeg for Segmentation: DeepMRSeg is used in the segmentation, which is train-

ing using CHBA. The CHBA is the integration of HBA and chronological concept.

- Proposed CJHBA-Based DRN for Classification: The classification is performed using the DRN classifier, which is trained using the proposed CJHBA. The proposed CJHBA is the integration of the Jaya algorithm, HBA, and chronological concept.

The remaining manuscript parts are structured as follows: Section 2 reviews previous studies related to segmentation and classification of tumors in the brain using MRIs, and Sect. 3 describes the proposed technique. The results and discussion of the techniques are described in Sect. 4. The research conclusion is provided in Sect. 5.

Motivation

The rapid increase of the cells in the brain is called brain tumor, which causes death if it is not treated well. The MRI is the most common method for brain structure analysis. There are many methods devised previously to effectively classify brain tumors. However, due to the various symptoms and structure of the tumor cells, the classification task is very difficult. The issues faced in the previously devised technique inspired us to develop a novel optimization technique for segmenting and classifying the tumors in the brain.

Literature Survey

The eight recent related techniques are reviewed in this part. Francisco Javier Díaz-Pernas et al. [6] implemented an automatic approach for segmenting and classifying the tumors in the brain. Here, the multiscale approach-based deep convolutional neural network was devised for identifying three kinds of tumors. It had good accuracy, and it was applicable to various imaging problems in the medical field. Anyhow, for larger datasets, this scheme was not appropriate. Yurong Guan et al. [5] implemented computer-assisted diagnosis (CAD) for the classification of tumors in the brain. Also, the agglomerative clustering-based scheme was employed for identifying the locations of the tumors. This scheme had less computational complexity and more accuracy. Furthermore, the data augmentation approach was employed in the reduction of over-fitting issues. However, the cost of computation was high for larger datasets. Jaeyong Kang et al. [2] developed transfer learning-based deep convolutional neural networks for better performance in segmentation and classification. Here, the best three deep features were evaluated, which gave to the classifier for improved performance. Thus, this ensemble feature-based classifier offered better performance for the larger dataset. Anyhow, real-time data analysis was difficult in this technique. Javaria Amin et al. [24] developed a CNN model for

efficiently classifying the tumor and non-tumor regions. Here, texture and structural information were fused, which was done using discrete wavelet transform (DWT) and Daubechies wavelet kernel. The segmentation was done using the global thresholding approach. This technique had good accuracy in segmentation, but the important features were not determined for the evaluation. Ahmad M. Sarhan [4] developed a CAD scheme for effective classification of the tumors in the brain. Here, DWT was applied for extraction of the required features and dimensionality reduction, which boosted the accuracy of the model. Also, this model was reliable and robust, but it required more time to complete the entire process. Isselmou Abd El Kader et al. [14] implemented a differential deep-CNN technique for identifying various brain tumor types using MRIs. Here, more differential feature maps were derived from the normal feature maps. Also, the contrast calculations of pixel directional patterns were used to improve the classification ability and accuracy. However, the minimum parameters were used, which may reduce the speed of coverage. Wadhah Ayadi et al. [25] implemented a support vector machine (SVM)-based technique to classify the cerebral tumors in the brain. In this approach, before classification, the normalization and feature extraction were carried out. The SVM classifier was used in the classification process, and the produced results were accurate with less computational time. Anyhow, robustness was less because of using less images modalities. Asmita Dixit and Aparajita Nanda [8] implemented an improved whale optimization algorithm (IWOA)-based radial basis neural network (RBNN) for classifying brain tumors. Here, the tumor area was identified using fuzzy-c means (FCM) clustering, and principle component analysis (PCA) was used in the feature extraction. This technique had high accuracy with less computational time. However, the tumor substructures were unable to detect in this technique.

Challenges

The issues that are identified in the previous brain tumor segmentation and classification techniques are listed as follows:

- The RBNN-IWOA technique obtained accurate classification results with less computational time, but the substructure identification of tumors was not possible [8].
- The identification of strong and meaningful features by the experts required more time, which led to errors during the handling of a large amount of data.
- The lesion complexity was another important drawback in the previous studies. Due to this complexity, early tumor identification and accuracy gets affected [25].
- The robustness of the system was affected due to the use of less modalities of the brain MRIs.

- Because of high intra- and inter-shape, contrast variations, and texture, the classification is difficult in the traditional approaches [2].

Proposed Chronological Jaya-Honey Badger Algorithm–Based Deep Residual Network for the Classification of Brain Tumors

This section shows the development procedure of the implemented brain tumor classification technique. The developed technique is useful in the early and exact identification of tumors in the brain, which leads to efficient treatment for patients. Therefore, in this research, an efficient optimization-enabled deep learning technique is developed for classifying and segmenting the tumors in the brain. The phases involved in the research are pre-processing, segmentation, feature extraction, data augmentation, and classification. Here, MRI is the input, which is given to the pre-processing phase for improving the image quality by removing the noises using normalization. Then, the DeepMRSeg [19] is used in the segmentation, which is training using CHBA. The CHBA is the integration of HBA and chronological concept. After segmenting, the CNN features [21] are extracted for proceeding the next step. Then, the data augmentation is achieved by means of randomized left or right flipping, rotation and brightness or contrast adjustment, random translation, and including Gaussian noise. After augmenting data, the classification is performed using DRN [22], in which the training is performed using the proposed CJHBA. The proposed CJHBA is the integration of the Jaya algorithm [23], HBA, and chronological concept. Figure 1 signifies the block diagram of the implemented model.

Data Acquisition

The data gathering happened in this step, and in the implemented technique, the brain MRIs are gathered from BRATS 2018 and Figshare datasets. Assume the dataset as O and the brain MRIs in the dataset are indicated as R and the notation is expressed as,

$$O = \{R_1, R_2, \dots, R_n, \dots, R_h\} \quad (1)$$

where the dataset is indicated as O , h is the entire MRIs in the dataset O , and R_n is the n th MRI in dataset O .

Pre-Processing

Pre-processing is the necessary step, which ensures performance enhancement by improving the quality of data. Also, in the deep learning-based model, noisy and unreliable data may affect the training time of the process, which is effectively handled using data pre-processing. Here, the normalization technique is used for pre-processing the

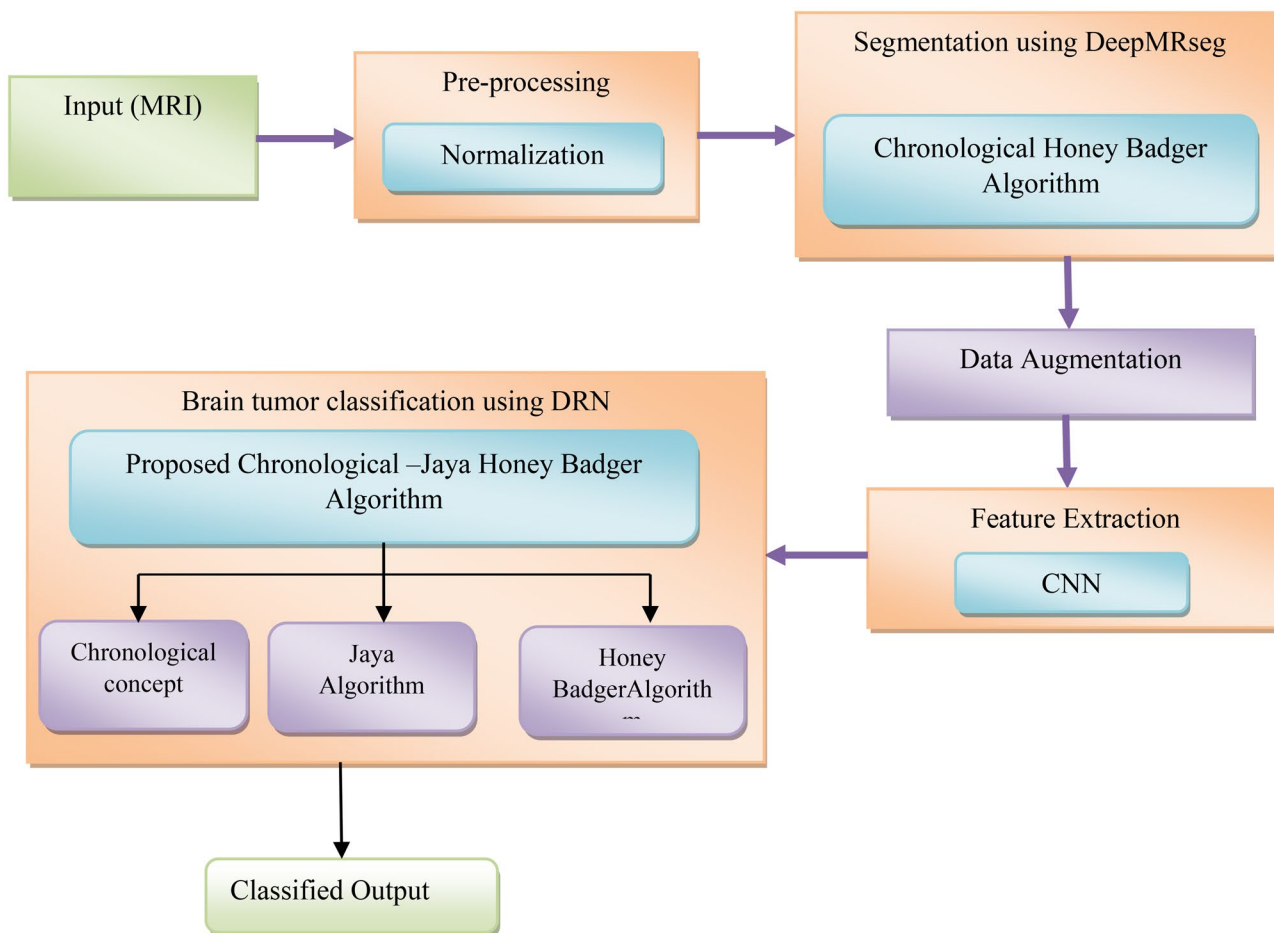


Fig. 1 Block diagram of the implemented model

input MRIs. The main aim of the normalization is to vary the pixel intensity values range, and it is useful to increase the contrast of the images. The other names of the normalization are histogram stretching or contrast stretching. The min–max normalization is used in this research to pre-process the input data. In this normalization approach, the maximum feature value is distorted into 1, the minimum value is distorted into 0, and for the other values the feature gets distorted into decimals in the range of 0 and 1. In the implemented model, every image Q_m is fed to pre-processing and the normalization [26] is given as,

$$z_j = \left(\frac{y_j - \min(y)}{\max(y) - \min(y)} \right) \quad (2)$$

where y_j is the position and j is varying as 1, 2, 3, ..., m , the intensity value of normalization against location y_j is denoted as z_j , and the maximum and minimum intensity values of all images are indicated as $\max(y)$ and $\min(y)$. The outcome of the pre-processing is signified as J_q , which is forwarded to further processing.

Brain Tumor Segmentation

The output of the pre-processing phase J_q is the input of DeepMRSeg, which is the segmentation classifier. For segmenting the tumors in the brain, the DeepMRSeg classifier is trained with the proposed CHBA.

DeepMRSeg Architecture

Figure 2 shows the structure of the DeepMRSeg classifier [19], in which J_q is the input of the classifier. It is a DL-related segmentation approach, which can be applicable of various types of segmentation tasks. Also, this classifier is mainly used in computer vision and healthcare image segmentation [19]. Here, the multi-scale features are extracted based on the consideration of sizes of multiple convolution filters using modified U-Net. This classifier is used in the effective segmentation of white matter lesion, deep structures of the brain, and hippocampus. The encoding and decoding are the two paths in the classifier. These paths are

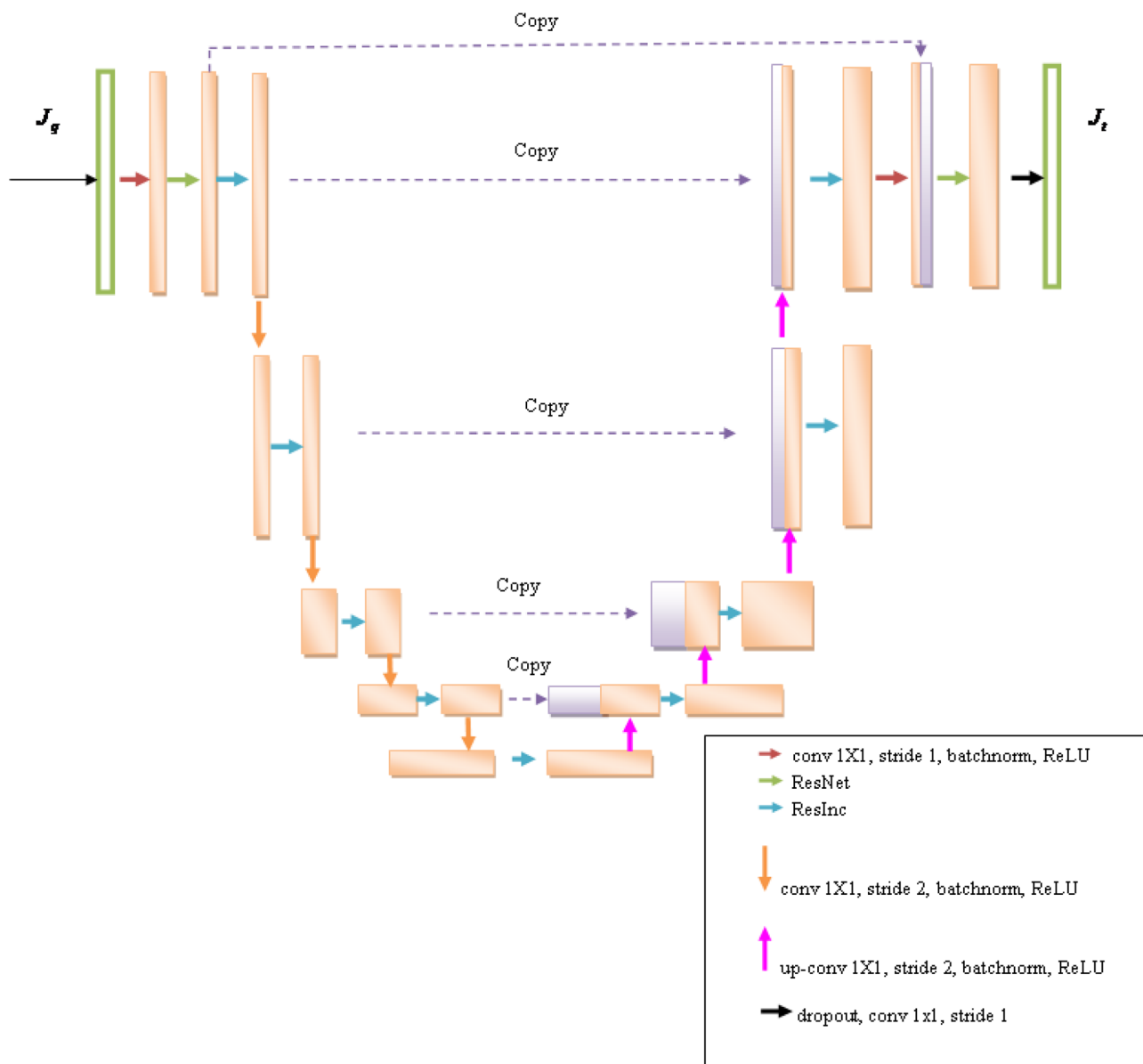


Fig. 2 Structure design of DeepMRSeg

present in U-Net after the multi-class soft-max and voxel-wise, which produce independent class probabilities of every voxel. The projection layer is the initial layer, which has a feature maps, and it is changed into desired amount of features b , which are fed to pre-encoding block, and it contains ResNet blocks. The extraction of numerous features from the input MRIs are done using ResNet, which creates the U-Net input. In the encoding path, the encode blocks are available. These blocks are useful in operating various resolutions of feature maps. In all the layers, the sub-samplings of features are done using the “transition down,” which is given to the ResInc block. When increasing the receptive field, the feature map sizes are decreasing in every layer. The decoding

section contains up-sampling operations along with ResInc blocks. The outcome of the segmentation process is J_t .

Deepmrseg Training Using Proposed CHBA

For effective tumor segmentation in the brains, the DeepMRSeg is trained using the proposed CHBA, and the CHBA is obtained by integrating the chronological concept with the HBA. The chronological concept is useful in the identification of how things vary over time and the historical details. The HBA [20] has the honey badger characteristics, which is a mammal variety with black and white fluffy fur. The prey

location is identified with the help of the smelling mouse skills. The two cases in the honey badger are digging mode and honey mode. In the digging mode, it utilizes the smelling capability to identify the prey location and choose the proper place for catching and digging the prey. In the honey mode, the honeyguide bird directly guides the location of the beehive. This algorithm is useful in solution making of the optimization challenges. Besides, it converges very fast and has a good exploration–exploitation balance. Therefore, integrating the chronological concept with HBA is useful in the effective segmentation of tumors in the brain. The algorithmic procedures of the CHBA are discussed below:

Step 1: Initialization

The entire honey badgers present in the population size is signified as P . The position of the population is given in the below equation.

$$c_k = od_k + u_1 \times (xd_k - od_k) \tag{3}$$

where the honey badger in k th location of the population is signified as c_k , and the search domain lower bound is denoted as od_k and search domain upper bounds is given as xd_k . The random number presents in 0 and 1 range is signified as u_1 .

Step 2: Fitness Evaluation

The best results are obtained using the fitness evaluation, in which the mean square error (MSE) is determined for obtaining the best solution. The minimum MSE is chosen as the best solution, and it is formulated as,

$$MSE = \frac{1}{h} \sum_{i=1}^h [\psi_i - J_i]^2 \tag{4}$$

where the expected output is symbolized as ψ_i and the output of DeepMRseg is denoted as J_i ; the total samples are given as h , such that $1 < i \leq h$.

Step 3: Describing Intensity (J)

The intensity is the major thing for identifying the concentration ability of the prey and the gap in between the k th honey and the prey. The smelling power of the prey is denoted as K_k . The inverse square law is used for describing the intensity. Based on this law, the intensity is defined as, when the smelling ability is high, then the prey moving speed is high; otherwise, speed of moving is slow. The intensity formula is denoted as,

$$K_k = u_2 \times \frac{V}{4\pi f_k^2} \tag{5}$$

where u_2 is the random number in 0 and 1 range. $V = (c_k - c_{k+1})^2$ and $f_k = c_{prey} - c_k$.

The source strength or the ability of concentration is denoted as U , and the space between the k th badger and prey is signified as f_k .

Step 4: Factor of Density Update

The density factor λ is used in the handling of time-varying randomization for guaranteeing the effortless exploration and exploitation moves. While minimizing the iterations, the density factor λ is minimized, and the density factor is calculated as,

$$\lambda = E \times \exp\left(\frac{-w}{w_{max}}\right) \tag{6}$$

where the total count of iterations is signified as w_{max} . The constant E is equal to or greater than 1. In general, the constant value E used is 2.

Step 5: Escaping from Local Optimum

The searching direction is modified based on the flag H , which has maximum choices for obtaining the scanning of search space for the search agents.

Step 6: Agent’s Position Update

The new location of the agent is denoted as c_{k+1} , and the location is divided into two, such as “honey phase” and “digging phase.”

Step 6.1: Digging Mode

The Cardioid shape function is useful for doing the operation in the digging mode, and the position update using the digging node is denoted as,

$$c_i(k+1) = c_{iprey} + H \times \alpha \times K \times c_{iprey} + H \times u_3 \times \lambda \times f_k \times \left| \cos(2\pi u_4) \times [1 - \cos(2\pi u_5)] \right| \tag{7}$$

where the best possible position is signified as c_k and the value of α is equal to or greater than 1. Most commonly, the value of α is denoted as 6. The food getting ability of the honey badger is indicated as α . The three random numbers are signified as u_3 , u_4 , and u_5 , which are in the range of 0 to 1. The flag H is determined based on the equation provided below.

$$H = \begin{cases} 1 & \text{if } u_6 \leq 0.5 \\ -1 & \text{else} \end{cases} \tag{8}$$

where u_6 is the random value in the range of 0 to 1. In digging mode, the honey badger smelling intensity J depends on the basis of the prey c_{prey} , and the density factor λ is influenced based upon the time. The need of better location of the prey is required when any disturbance occurs in the digging mode.

Step 6.2: Honey Mode

The food identification of honey badger happens due to the use of honeyguide bird is called the honey mode, and the formula for obtaining this step is,

$$c_l(k + 1) = c_{lprey} + H \times u_7 \times \lambda \times f_k \tag{9}$$

$$f_k = c_{prey} - c_l(k) \tag{10}$$

When substituting Eq. (10) in Eq. (9),

$$c_l(k + 1) = c_{prey} + H \times u_7 \times \lambda \times (c_{prey} - c_l(k)) \tag{11}$$

$$c_l(k + 1) = c_{prey} + H \times u_7 \times \lambda \times c_{prey} - H \times u_7 \times \lambda \times c_l(k) \tag{12}$$

$$c_l(k + 1) = c_{prey} [1 + H \times u_7 \times \lambda] - H \times u_7 \times \lambda \times c_l(k) \tag{13}$$

The equation for the chronological concept is given as,

$$c_l(k + 1) = \frac{c_l(k + 1) + c_l(k + 1)}{2} \tag{14}$$

When the iteration is k

$$c_l(k) = c_{prey} [1 + H \times u_7 \times \lambda] - H \times u_7 \times \lambda \times c_l(k) \tag{15}$$

When substituting Eq. (15) in Eq. (13),

$$c_l(k + 1) = c_{prey} [1 + H \times u_7 \times \lambda] - H \times u_7 \times \lambda [c_{prey} (1 + H \times r_7 \times \lambda) - H \times u_7 \times \lambda \times c_l(k + 1)] \tag{16}$$

$$c_l(k + 1) = c_{prey} [1 + H \times u_7 \times \lambda] - H \times u_7 \times \lambda [c_{prey} (1 + H \times r_7 \times \lambda) + c_l(k - 1)H^2 \times u_7^2 \times \lambda^2] \tag{17}$$

$$c_l(k + 1) = c_{prey} (1 + H \times u_7 \times \lambda) [1 - H \times u_7 \times \lambda] + c_l(k - 1)H^2 \times u_7^2 \times \lambda^2 \tag{18}$$

When substituting Eqs. (18) and (13) in Eq. (14),

$$c_l(k + 1) = \frac{c_{prey} [1 + H \times u_7 \times \lambda] - H \times u_7 \times \lambda \times c_l(k) - c_l(k) (1 + H \times u_7 \times \lambda) [1 - H \times u_7 \times \lambda] + c_l(k - 1)H^2 \times u_7^2 \times \lambda^2}{2} \tag{19}$$

$$c_l(k + 1) = \frac{c_{prey} (1 + H \times u_7 \times \lambda) [1 + (1 - H \times u_7 \times \lambda)] - c_l(k)H \times u_7 \times \lambda + c_l(k - 1)H^2 \times u_7^2 \times \lambda^2}{2} \tag{20}$$

Pseudo code of CHBA
Parameters w_{max}, P, λ, E
Fitness evaluation using Equation (4)
Saving the optimal position c_{prey}
while $k \leq k_{max}$ do
Modify λ (decreasing factor) by Equation (6).
for $k = 1$ to P do
Determining Intensity K_i by Equation (5).
if $u < 0.5$ then
Location update $c_l(k + 1)$ by Equation (7).
Else
Location update $c_l(k + 1)$ by Equation (9).
end if
Re-evaluate the fitness function
End while for obtaining maximum iteration
Return best solution
Terminate

Algorithm 1 Pseudo-code of devised CHBA

$$c_l(k + 1) = \frac{1}{2} [c_{prey} (1 + H \times u_7 \times \lambda) (2 - H \times u_7 \times \lambda) - c_l(k)H \times u_7 \times \lambda + c_l(k - 1)H^2 \times u_7^2 \times \lambda^2] \tag{22}$$

where $c_l(k + 1)$ denotes the l th solution at iteration $k + 1$, $c_l(k)$ denotes the l th solution at iteration k , $c_l(k - 1)$ denotes the l th solution at iteration $k - 1$, and the location of the prey is specified as c_{prey} .

Step 7: Re-evaluation of Fitness

After obtaining the update in Eq. (22), again, the fitness value is evaluated for choosing the best results.

Step 8: Termination

The algorithm is terminated, when obtaining the maximum number of iteration k_{max} . Algorithm 1 denotes the pseudo-code of devised CHBA.

Data Augmentation

Data augmentation is useful in increasing the amount of data by including slightly modified already existing data copies or creating imitation data newly from previously available data. The data augmentation plays the responsibility of the regularizer and is helpful in the reduction of overfitting

$$c_l(k + 1) = \frac{1}{2} [c_{prey} (1 + H \times u_7 \times \lambda) [1 + (1 - H \times u_7 \times \lambda)] - c_l(k)H \times u_7 \times \lambda + c_l(k - 1)H^2 \times u_7^2 \times \lambda^2] \tag{21}$$

during the training of the classifier. The segmentation outcome J_i is considered as the input of data augmentation. The augmented outcome is obtained using flipping of image,

translation of image, rotation of image, noise added image, and brightness. In flipping, the image orientation is flipped in the vertical or horizontal direction, and the outcome is denoted as J_g . The translated image is obtained by moving the image in various directions, and J_u is the translated image outcome. The image is rotated in a particular degree that is called rotated image, and J_s is used to represent the result of the rotated image. To obtain more training data, noises are added in the image and the output of noise added image is denoted as J_o . The image contrast is improved in brightness, and the output is indicated as J_d . The data augmentation outcome is provided as $R_i = \{J_t, J_g, J_u, J_s, J_o, J_d\}$.

Extracting the Feature

The feature extraction is the process of reducing the dimension of the image. Here, to do the process in an easy manner, the raw input data is classified into various groups. In general, large datasets require more variables and a large number of computing resources, so that the optimal features are extracted. Besides, in this process, the dimension of the data was highly reduced, which will enhance the accuracy of the model. In the devised model, the CNN features are selected for the data augmentation. The CNN features [21] are denoted as $G = \{g_1, g_2, \dots, g_r\}$. The CNN is a variety of artificial neural network, which is commonly devised for extracting the features and for classifying the high dimensional data. Also, it is useful in reorganizing the two-dimensional shapes with scaling, translation, distortion, and skewing functions. The processes involved in the CNN are extracting the features, mapping of features, and layers sub-sampling. The various layers present in the CNN are convolutional, sub-sampling layers, and fully connected output layers. The backpropagation algorithm is applied for training the CNN model. Figure 3 represents the CNN feature extraction.

Tumor Classification in Brain Using the Proposed CJHBA-Based DRN

The tumors in the brain are classified using the CNN features G , which are provided as the input to the DRN classifier. The tumors in the brain are classified using implemented CJHBA-based DRN, in which the weights and biases of the DRN are trained by the implemented CJHBA.

DRN Architecture

The DRN classifier [22] is mainly used in image recognition and pattern recognition tasks. When compared with other deep learning techniques, the DRN has maximum speed for training, and simple gradient transmission. Also, it obtains good results in classification and regression tasks. Moreover, the computational efficiency of this classifier is high, and it avoids overfitting issues.

Convolutional Layer In the deep learning methods, the general 2D convolutional layer (Conv2d) is applied for reducing the free parameters used for training procedure. Also, it has the advantage of weight sharing in the local receptive field. Here, filter series are called kernel that is used in for processing the input. The process of the convolutional layer is given as,

$$I2d(G) = \sum_{y=0}^{F-1} \sum_{z=0}^{F-1} U_{y,z} \cdot G_{(c+y),(d+z)} \tag{23}$$

$$I1d(G) = \sum_{s=0}^{C_{in}-1} S_s * G \tag{24}$$

where the input image of the convolutional layer is denoted as I ; the coordinates used for recoding is signified as c and d ;

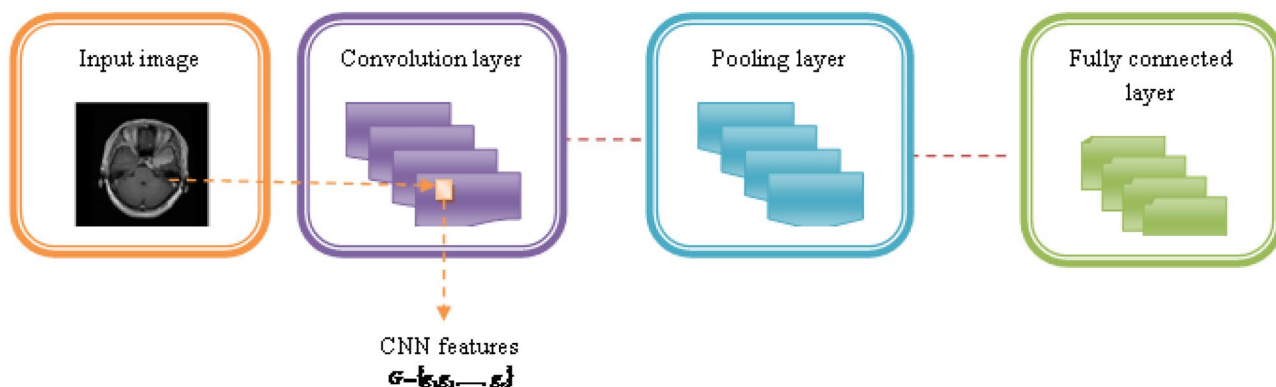


Fig. 3 Extraction of CNN features

$F \times F$ kernel matrix is represented as, which is also referred as a learnable parameter; and the kernel matrix location index is denoted as y and z . Therefore, sth input neuron kernel size is denoted as and the cross-correlation operator is denoted as $*$.

Pooling Layer This layer is used to control the over fitting issues and minimize the feature map’s spatial size. This layer is presents next to the convolutional layer. Here, the average pooling is selected, which is used for operating on every feature map size, and all the values are replaced by the average pooling.

$$y_{out} = \frac{y_{in} - S_y}{\eta} + 1 \tag{25}$$

$$z_{out} = \frac{z_{in} - S_z}{\eta} + 1 \tag{26}$$

where the width and height of the input matrix are signified as y_{in} and z_{in} , the outcome of input matrix width and height are y_{out} and z_{out} , and the kernel size width and height are signified as S_y and S_z .

Activation Function The complex and non-linear features are educated using the activation function, so that it is useful in the enhancement of mined features non-linearity, which is used for the MRI processing that is rectified linear unit (ReLU) and which is given below,

$$Re\ LU(G) = \begin{cases} 0; L < 0 \\ L; L \geq 0 \end{cases} \tag{27}$$

Batch Normalization In the deep learning techniques, to obtain a better tradeoff among the computation complexity and convergence, the data used for training is divided into more small divisions known as mini-batches and the training is achieved based on these mini-batches. Here, the normalization is carried out in input layers using the activations alteration and scaling for increasing the consistency and speediness of training.

Residual Blocks It is the shortcut association in-between the output and input of a residual block. If the size of the residual block input and output are identical, then the output and input are directly linked with each other. Else, the dimension matching factor is required for linking the input and output.

$$B = v(G) + G \tag{28}$$

$$B = v(G) + \varpi_G G \tag{29}$$

where input is the feature, which is denoted as G , the output of the residual block is indicated as B , the mapping relationship is indicated as v , and ϖ_G signifies the dimension matching factor.

Linear Classifier: It is used in the determination of the classification outputs. It is the grouping of softmax function and fully connected (FC) layer. The operation of the FC layer is the same as multi-layer perceptron, in which the neurons are linked to each other in various layers. The softmax activation function is utilized in the normalization of the input vector into a probability vector and the highest probability class is the final result.

$$T = \delta B + \zeta \tag{30}$$

Here, δ indicates the weight matrix, the bias is indicated as ζ , and T signifies the DRN output. Figure 4 represents the architectural design of DRN.

DRN Training Using the Developed CJHBA

The DRN classifier is trained using the proposed hybrid optimization approach namely CJHBA, in which the weight and bias of the classifier are trained with developed CJHBA for determining the optimum solution. The implemented CJHBA is the integration of chronological concept, Jaya, and HBA. The historical details related to things, which are changing based on time, are identified using the chronological concept. The HBA is useful in the solution-making of the optimization challenges. Besides, it converges very fast and has a good exploration–exploitation balance. In the Jaya algorithm, there is no need of algorithm-specific parameters and the simple general parameters are used for optimization. Because of this benefit, this algorithm is useful in solving various real-world optimization issues, like automatic clustering, mechanical design issues, and optimum power flow. However, it is difficult for doing complex multi-dimensional issues, which lead to slow convergence. Hence, integrating the chronological concept, HBA, with the Jaya algorithm is useful in the effective classification of tumors in the brain. The steps are discussed below:

Fitness Evaluation To determine the fitness, the mean square error (MSE) is evaluated for every solution, and the solution with minimum MSE is considered the optimal solution. The formula used for the fitness evaluation is given as,

$$MSE = \frac{1}{h} \sum_{i=1}^h [\xi_i - T]^2 \tag{31}$$

where the expected output of DRN is symbolized as ξ_i and the original output of DRN is indicated as T , and h signifies the total samples and $1 < i \leq h$.

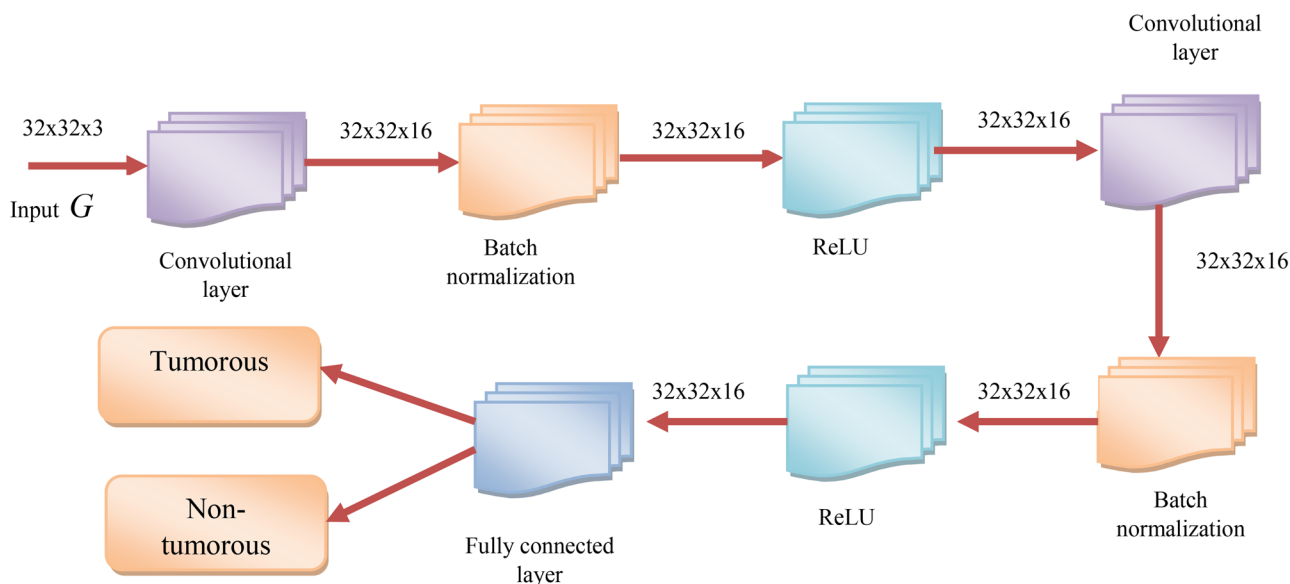


Fig. 4 DRN architecture

Let us consider Eq. (22), which is the hybridization of the chronological concept and HBA. Along with this, the Jaya algorithm is integrated to obtain the proposed CJHBA, and the steps in the Jaya algorithm is given as,

$$c_l(k + 1) = c_l(k) + w_1(k)(c_{best}(k) - c_l(k) - w_2(k)(c_{worst}(k) - c_l(k))) \tag{32}$$

$$c_l(k + 1) = c_l(k) + w_1(k)(c_{best}(k) - w_1(t)v_l(k) - w_2(k)(c_{worst}(k) - w_2(k)c_l(k))) \tag{33}$$

$$c_l(k + 1) = c_l(k)[1 - w_1(k) + w_2(k)] + w_1(k)c_{best}(k) - w_2(k)c_{worst}(k) \tag{34}$$

$$c_l(k)[1 - w_1(k) + w_2(k)] = c_l(k + 1) - w_1(k)c_{best}(k) - w_2(k)c_{worst}(k) \tag{35}$$

$$c_l(k) = \frac{c_l(k + 1) - w_1(k)c_{best}(k) - w_2(k)c_{worst}(k)}{[1 - w_1(k) + w_2(k)]} \tag{36}$$

While substituting Eq. (35) in Eq. (21),

$$c_l(k + 1) = \frac{1}{2} [c_{prey}(1 + H \times u_7 \times \lambda)(2 - H \times u_7 \times \lambda) - \left(\frac{c_l(k + 1) - w_1(k)c_{best}(k) - w_2(k)c_{worst}(k)}{[1 - w_1(k) + w_2(k)]} \right) (H \times u_7 \times \lambda) + c_l(k - 1)H^2 \times u_7^2 \times \lambda^2] \tag{37}$$

$$c_l(k + 1) + \frac{c(k + 1)H \times u_7 \times \lambda}{2[1 - w_1(k) + w_2(k)]} = \frac{1}{2} [c_{prey}(1 + H \times u_7 \times \lambda)(2 - H \times u_7 \times \lambda) - \left(\frac{c_l(k + 1) - w_1(k)c_{best}(k) - w_2(k)c_{worst}(k)}{[1 - w_1(k) + w_2(k)]} \right) (H \times u_7 \times \lambda) + c_l(k - 1)H^2 \times u_7^2 \times \lambda^2] \tag{38}$$

$$\frac{c_l(k + 1)2[1 - w_1(k) + w_2(k)] + c(k + 1)H \times u_7 \times \lambda}{2[1 - w_1(k) + w_2(k)]} = \frac{1}{2} \left[\begin{aligned} &c_{prey}(1 + H \times u_7 \times \lambda)(2 - H \times u_7 \times \lambda) \\ &- \left(\frac{c_l(k + 1) - w_1(k)c_{best}(k) - w_2(k)c_{worst}(k)}{[1 - w_1(k) + w_2(k)]} \right) (H \times u_7 \times \lambda) + \\ &c_l(k - 1)H^2 \times u_7^2 \times \lambda^2 \end{aligned} \right] \tag{39}$$

$$c_l(k + 1) \left[\frac{2[1 - w_1(k) + w_2(k)] + H \times u_7 \times \lambda}{2[1 - w_1(k) + w_2(k)]} \right] = \frac{1}{2} [c_{prey}(1 + H \times u_7 \times \lambda)(2 - H \times u_7 \times \lambda) - \left(\frac{c_l(k + 1) - w_1(k)c_{best}(k) - w_2(k)c_{worst}(k)}{[1 - w_1(k) + w_2(k)]} \right) (H \times u_7 \times \lambda) + c_l(k - 1)H^2 \times u_7^2 \times \lambda^2] \tag{40}$$

Pseudo code of CJHBA	
Parameters	w_{min}, P, λ, E
Evaluating the fitness using Equation (30)	
Store best location c_{prey}	
while $k \leq k_{max}$ do	
Modify the decreasing factor λ using Eqn. (5).	
for $k = 1$ to P do	
Intensity K_i determination using Eqn. (4).	
if $u < 0.5$ then	
Location update $c_i(k+1)$ by Eqn. (6).	
else	
Location update $c_i(k+1)$ by Eqn. (8).	
end if	
Obtain the chronological concept using Eqn. (13).	
Evaluate the best solution using Eqn. (21)	
Obtain the Jaya algorithm using Eqn. (31).	
New position evaluation using Eqn. (40)	
End for	
End while when satisfying the stopping criteria.	
Return best solution	
Terminate	

Algorithm 2 Proposed CJHBA pseudo-code

The final equation is

$$c_l(k+1) = \left[c_{prey} (1 + H \times u_7 \times \lambda) (2 - H \times u_7 \times \lambda) - \left(\frac{c_l(k+1) - w_1(k)c_{best}(k) - w_2(k)c_{worst}(k)}{[1 - w_1(k) + w_2(k)]} \right) (H \times u_7 \times \lambda) + c_l(k-1)H^2 \times u_7^2 \times \lambda^2 \right] * \left[\frac{[1 - w_1(k) + w_2(k)] + H \times u_7 \times \lambda}{2[1 - w_1(k) + w_2(k)]} \right] \tag{41}$$

The algorithm is terminated when satisfying the stopping criteria. The pseudo-code of the devised CJHBA is discussed in Algorithm 2.

Thus, the tumorous or non-tumorous are determined by the integration of chronological concept, HBA, and Jaya algorithm.

Results and Discussion

This section contains the details regarding the experimentation and discussion of the implemented CJHBA-based DRN. The setup details, dataset description, metrics, and results details are explained in further sections.

Experimental Setup

The experimentation of the implemented CJHBA-based DRN is determined using MATLAB with windows 10 OS, 4 GB RAM, and Intel i3 processor.

Dataset Description

The efficiency of the implemented CJHBA-based DRN is evaluated using two datasets, such as BRATS 2018 [27] and Figshare dataset [28].

BRATS 2018 Dataset (dataset-A) This dataset contains the MRI scans of pre-operative brain tumors obtained from multi-institution. Also, it concentrates on the intrinsic heterogeneous segmentation of brain tumors (in histology, shape, and appearance) called gliomas. Moreover, this dataset is used to pinpoint the medical relationship of segmentation and concentrates the overall survival prediction using radiomic features integrative analyzes and machine learning algorithms.

Figshare Dataset (dataset-B) It is a dataset for brain tumors with 3064 T1-weighted contrast-enhanced images. Also, it contains brain tumor types as glioma, meningioma, and pituitary. Here, 930 slices are available in pituitary tumor, 1426 slices available in 1426 glioma, and 708 slices are available in meningioma.

Performance Metrics

The testing accuracy, specificity, sensitivity, and receiver operating characteristic (ROC) curve metrics are considered for evaluating the implemented scheme.

Accuracy: It is defined as how well the implemented brain tumor classification method is correctly classified, and it is formulated as,

$$Accuracy = \frac{TPos + TNeg}{FNeg + FPos + TPos + TNeg} \tag{42}$$

where true negative, true positive, false negative, and false positive are denoted as $TNeg$, $TPos$, $FNeg$, and $FPos$, respectively.

Specificity It is determined as the proportion of correct identification of true negatives, and the formula is given as,

$$Specificity = \frac{TNeg}{TNeg + FPos} \tag{43}$$

Sensitivity It is determined as the proportion of correct identification of true positives, and the formula is given as,

$$Sensitivity = \frac{TPos}{TPos + FNeg} \tag{44}$$

ROC It is the classification aptitude of the proposed brain tumor classification system. It is plotted true positive rate (TPR) against the true negative rate (TNR) based on various threshold settings.

Experimental Results

The experimental results using dataset-A (three images) are given in Fig. 5. The input MRIs are represented in

Fig. 5 Experimental results using dataset-A: **a** input images, **b** pre-processed images, **c** segmented images, **d** flipped images, **e** rotated images, **f** translated images, and **g** noised added images

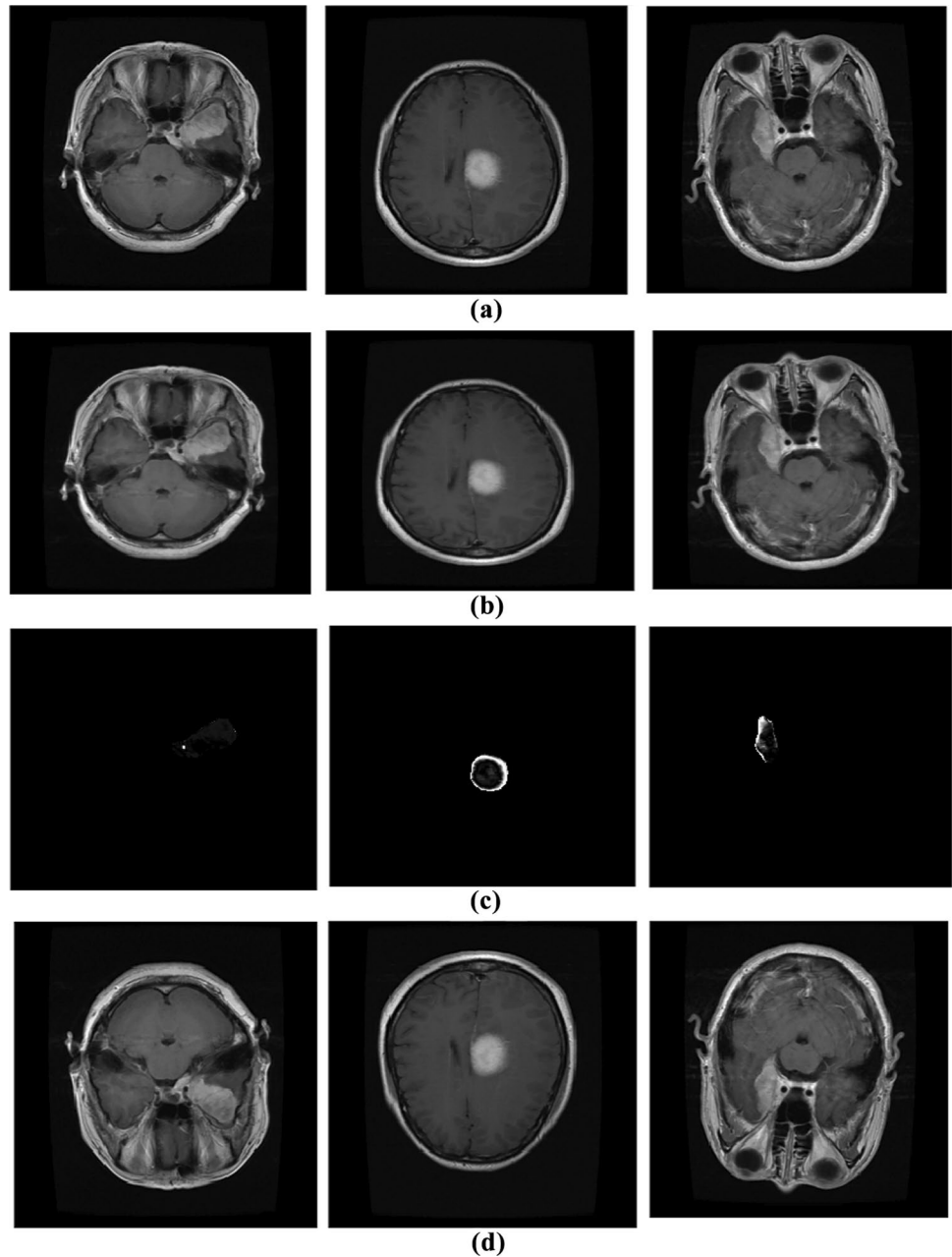


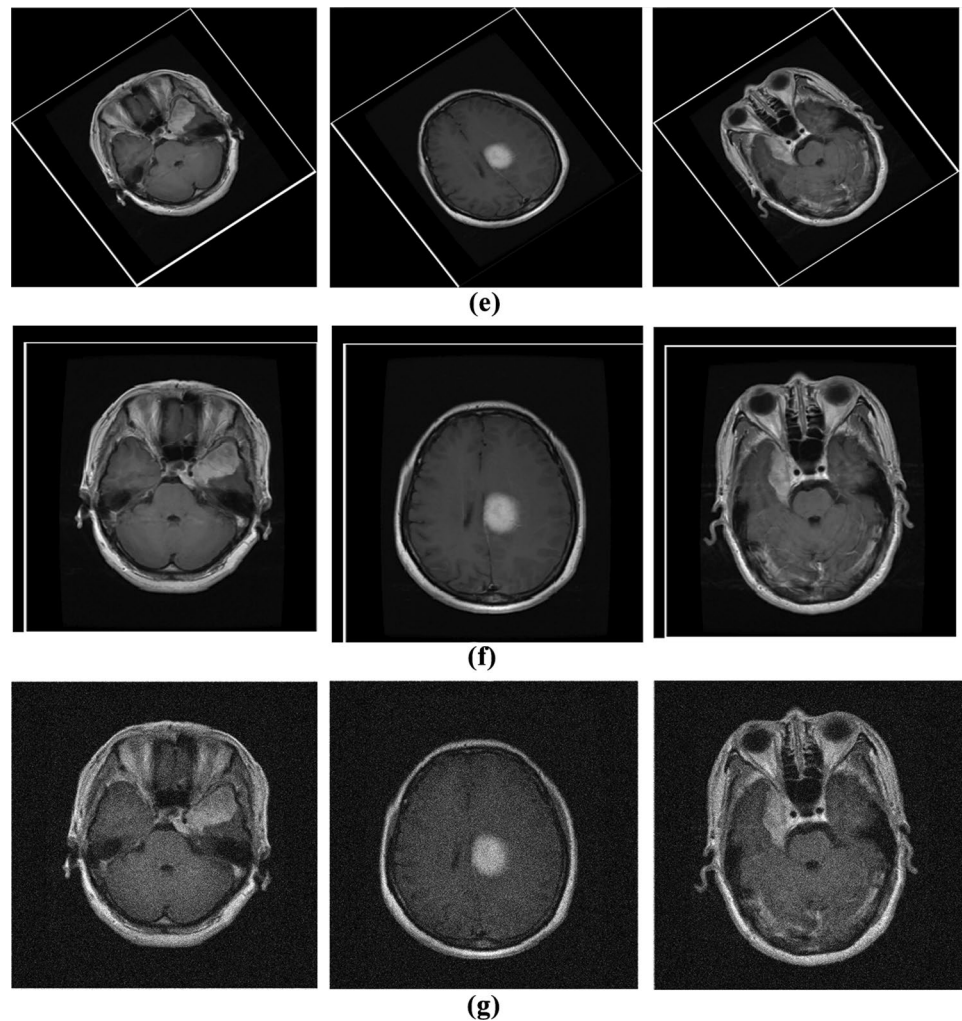
Fig. 5a, and the pre-processed results are provided in Fig. 5b. Then, the segmented MRIs are given in Fig. 5c. The augmented results, such as flipped, are given in Fig. 5d, rotated is provided in Fig. 5e, translated is given in Fig. 5f, and noise added images are provided Fig. 5g.

Figure 6 represents the experimental results using dataset-B (three images). The input MRIs is represented in Fig. 6a, and the pre-processed results are provided in Fig. 6b. Then, the segmented MRIs are given in Fig. 6c. The augmented results, such as flipped, are given in Fig. 6d, rotated is provided in Fig. 6e, translated is given in Fig. 6f, and noise added images are provided Fig. 6g.

Segmentation Analysis

The segmentation accuracy is analyzed using dataset-A and dataset-B, which is depicted in Fig. 7. The segmentation accuracy of using dataset-A is shown in Fig. 7a, which is evaluated by varying the training data. The comparison methods used for evaluating the segmentation accuracy of the implemented DeepMRseg are SegNet, U_net, and DeepJoint. When the training data = 70%, the segmentation accuracy of the methods SegNet, U_net, and DeepJoint, and implemented DeepMRseg is 0.8289, 0.8578, 0.8630, and 0.9052, respectively. The segmentation accuracy of the

Fig. 5 (continued)



DeepMRseg is more because of the training of the DeepMRseg with the hybrid optimization technique CHBA. Similarly, the segmentation accuracy of implemented DeepMRseg that is determined using dataset-B is given in Fig. 7b. For training data = 60%, the segmentation accuracy of the implemented DeepMRseg is 0.9023, whereas SegNet, U_net, and DeepJoint obtain the segmentation accuracy of 0.8405, 0.8517, and 0.8842, respectively. When increasing the percentage of training data, the segmentation accuracy improves, and the maximum accuracy is achieved at 90% training data.

Comparative Methods

The classification performance of the implemented CJHBA-based DRN is compared with previously implemented techniques, such as transfer learning [26], Bayesian fuzzy clustering (BFC) [29], deep neural network (DNN) [30], and CNN [31].

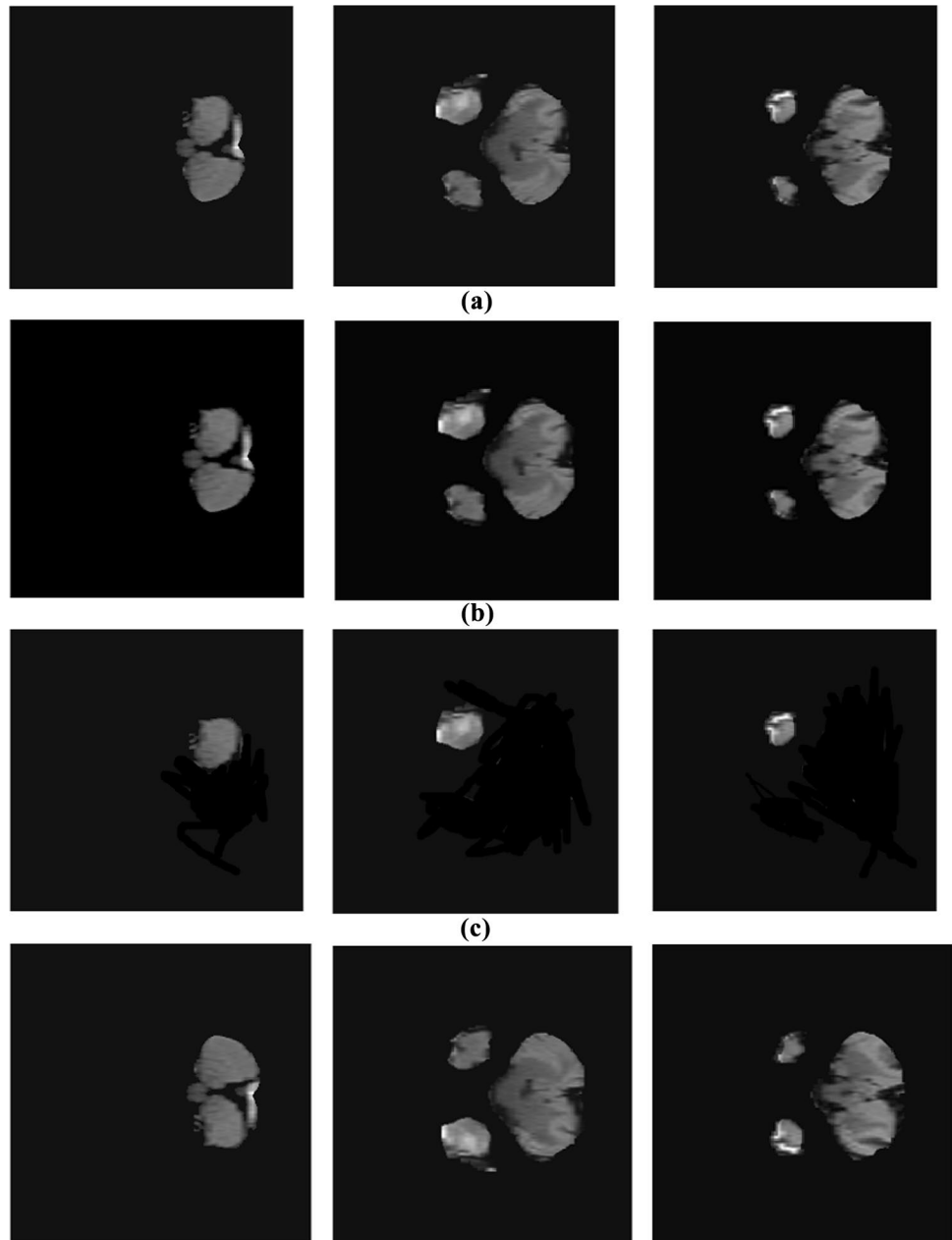
Comparative Analysis

The classification performance of the implemented technique is evaluated using two datasets, which are discussed below.

Comparative Analysis using Dataset-A

The classification performance of the implemented CJHBA-based DRN using dataset-A is resulted in Fig. 8. The analysis is based on adjusting the training percentage to examine accuracy, specificity, sensitivity, and ROC. The testing accuracy evaluation is shown in Fig. 8a. The accuracy of the implemented CJHBA-based DRN is 0.8934, for 60% of training data. For the same training percentage, the transfer learning, BFC, DNN, and CNN methods have the accuracy of 0.8211, 0.8322, 0.8433, and 0.8754, respectively. Figure 8b shows the sensitivity analysis of the model. When 70% of training data is used

Fig. 6 Experimental results using dataset-B: **a** input images, **b** pre-processed images, **c** segmented images, **d** flipped images, **e** rotated images, **f** translated images, and **g** noised added images



for the evaluation, the proposed method offers a sensitivity of 0.9089, and the improvement percentage with transfer learning is 5.02%, BFC is 3.84%, DNN is 3.07%, and CNN is 2.94%. The specificity analysis is depicted in Fig. 8c. The specificity of the models, such as transfer learning, BFC, DNN, CNN, and implemented CJHBA-based DRN are 0.8682, 0.8838, 0.8983, 0.9075, and 0.9239, respectively, for 80% of training data. The ROC analysis is given in Fig. 8d, in which the TPR is plotted against the FPR. When TPR is 0.4, the FPR of the models, such as transfer learning, BFC, DNN, CNN, and implemented CJHBA-based DRN, are 0.7968, 0.8124, 0.8699, 0.8515, and 0.8728, respectively. By considering the classification

performance analysis, the developed CJHBA-based DRN has attained maximum performance at 90% training data, which is happened due the effective training of the DRN classifier with the implemented CJHBA.

Comparative Analysis Using Dataset-B

Figure 9 shows the classification performance of the implemented CJHBA-based DRN using dataset-B. The analysis is based on adjusting the training percentage to examine accuracy, specificity, sensitivity, and ROC. The testing accuracy determination is depicted in Fig. 9a. The testing accuracy of transfer learning, BFC, DNN, CNN, and

Fig. 6 (continued)

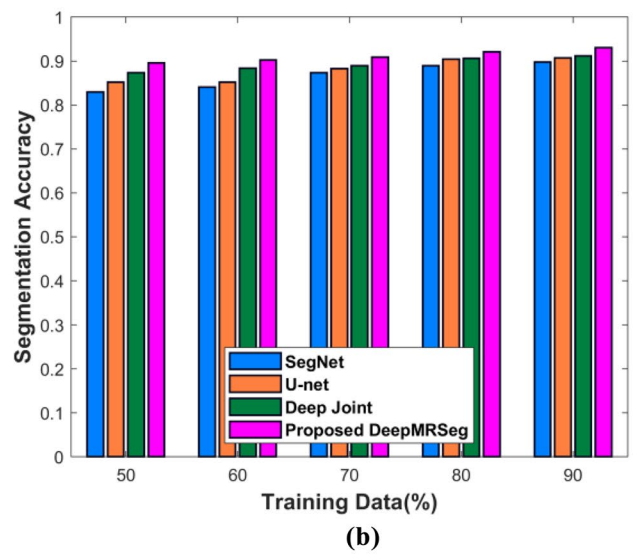
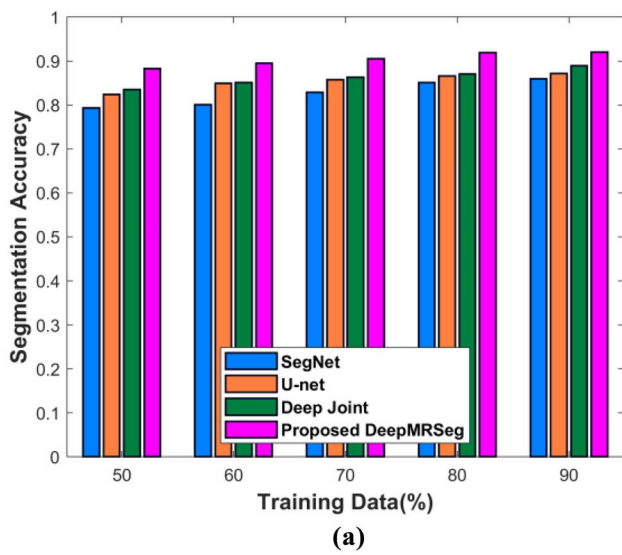
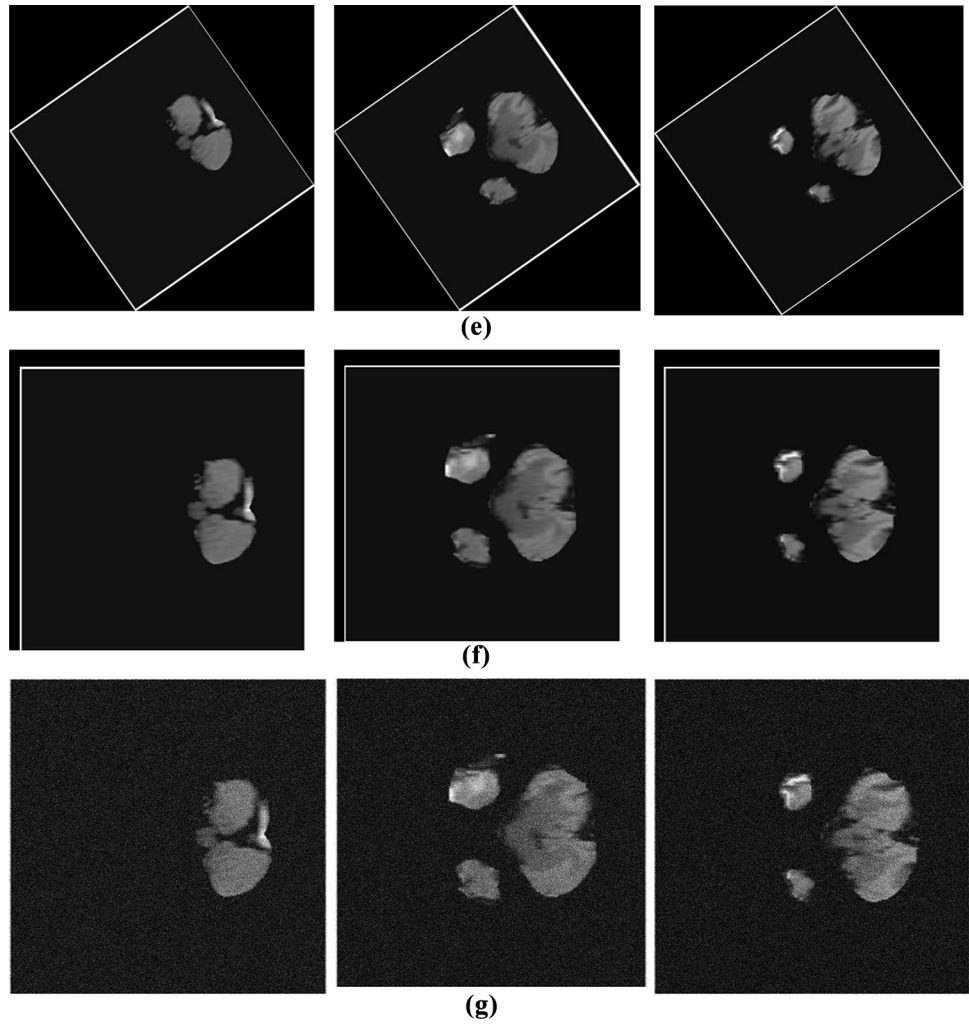


Fig. 7 Analysis based on segmentation accuracy: **a** dataset-A and **b** dataset-B

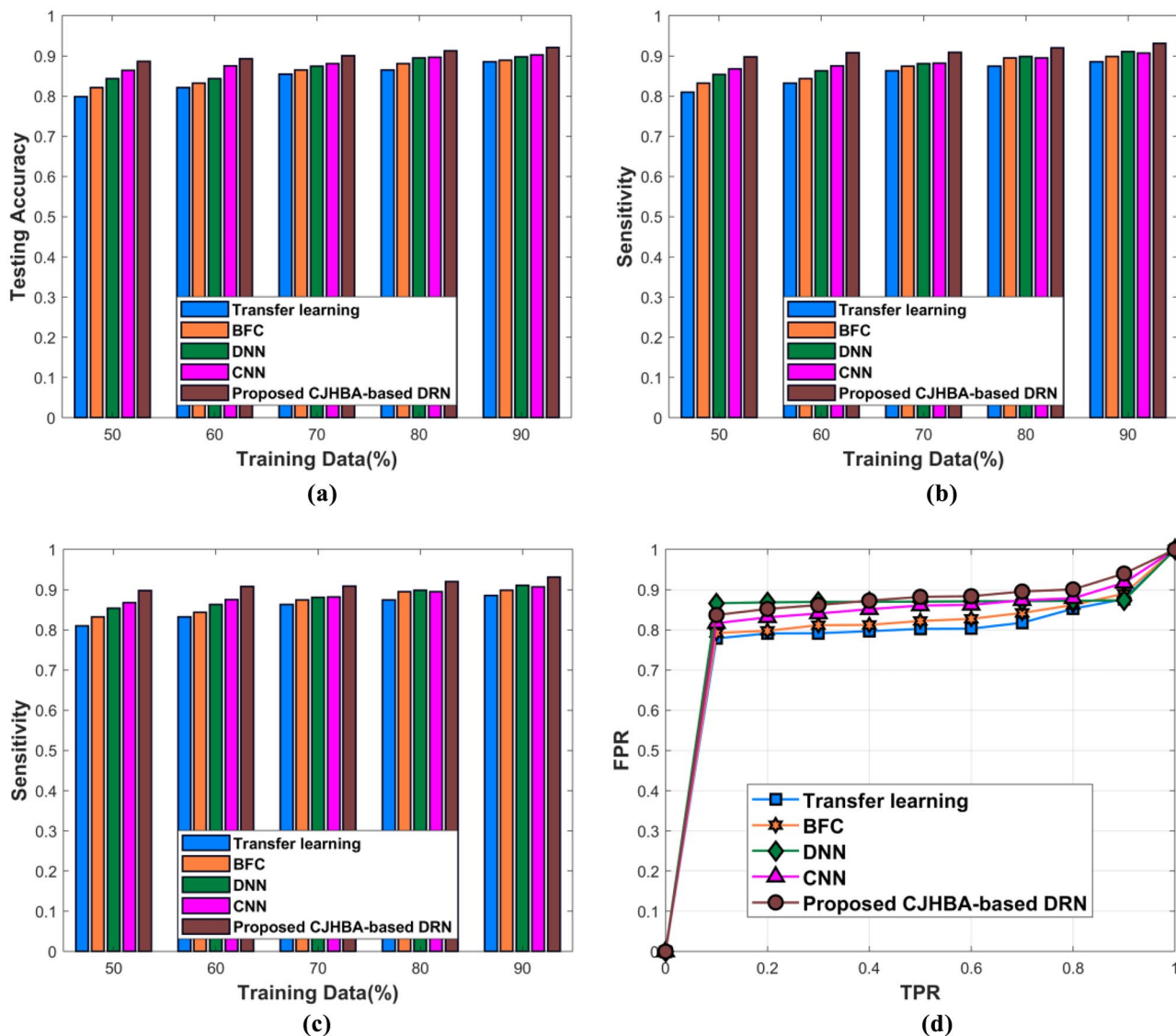


Fig. 8 Comparative analysis using dataset-A: a accuracy, b sensitivity, and c specificity

implemented CJHBA-based DRN methods are 0.7949, 0.8284, 0.8584, 0.8731, and 0.9110, respectively, for 80% of training data. The sensitivity evaluation is shown in Fig. 9b. When evaluating the sensitivity, the sensitivity of the implemented approach is 0.9043, for 60% of training data. For the same training percentage, the transfer learning, BFC, DNN, and CNN methods have a sensitivity of 0.7954, 0.8190, 0.8231, and 0.8640, respectively. Figure 9c shows the specificity analysis of the model. When 70% of training data is considered for the evaluation, the proposed method offers the specificity of 0.9109, which is 11.27% improved than transfer learning, 7.80% improved than BFC, 9.08% improved than DNN, and 3.44% improved than CNN. Figure 9d shows the ROC analysis. The FPR of

transfer learning is 0.8823, BFC is 0.8809, DNN is 0.8876, CNN is 0.8612, and implemented approach is 0.8976, respectively, for considering the TPR as 0.6. The classification performance is enhanced because of the hybridization of the chronological concept, Jaya algorithm, and HBA.

Algorithmic Analysis

The algorithmic analysis is carried out to show the efficiency of implemented CJHBA + DRN with other optimization algorithms. Here, the optimization algorithms considered for the evaluation are Competitive swarm optimization (CSO) + DRN, JOA + DRN, HBA + DRN, and proposed CJHBA + DRN.

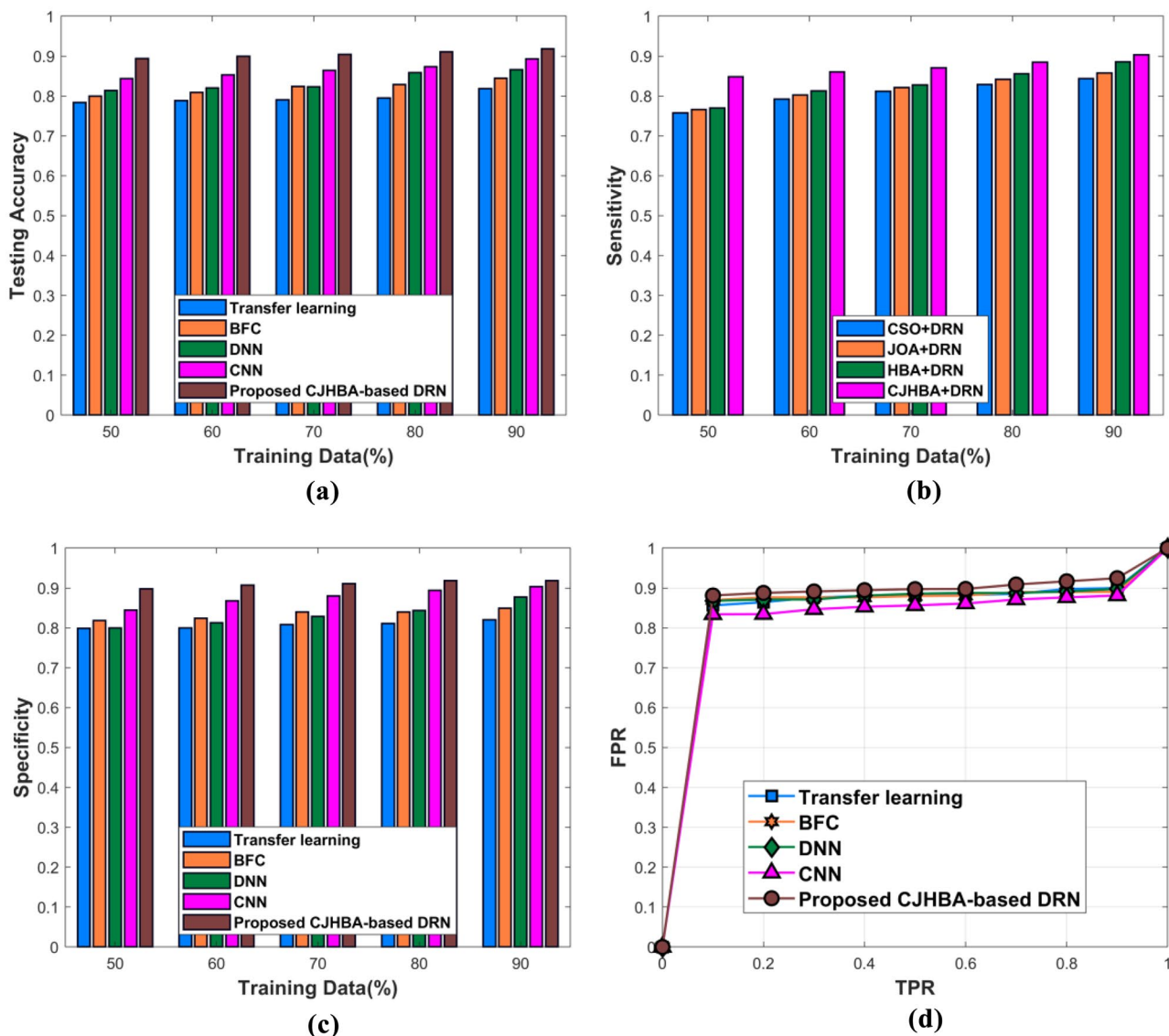


Fig. 9 Comparative analysis using dataset-B: a accuracy, b sensitivity, c specificity, and d ROC

Algorithmic Analysis Using Dataset-A

The algorithmic analysis using dataset-A is shown in Fig. 10. The evaluation is done using various metrics. The algorithmic analysis of accuracy is depicted in Fig. 10a by varying the training data. When 70% of training data is used for evaluation, the accuracy of the methods, such as CSO + DRN, JOA + DRN, HBA + DRN, and implemented CJHBA + DRN, are 0.8594, 0.8713, 0.8788, and 0.8898, respectively. Similarly, the sensitivity and specificity algorithmic analysis are given in Fig. 10b, c, respectively. In the sensitivity analysis, for 80% of training data, the sensitivity of the implemented CJHBA + DRN is 0.9038, and other methods, such as CSO + DRN, JOA + DRN, and HBA + DRN, are 0.8726, 0.8837, and 0.8868, respectively. In the same

way, for the same training percentage, the specificity of the CJHBA + DRN is 0.9061, whereas the CSO + DRN is 0.8749, JOA + DRN is 0.8860, and HBA + DRN is 0.8891. By the consideration of dataset-A, the implemented algorithm shows the effective outcomes, which is because of the hybridization of the chronological concept, Jaya algorithm, and HBA.

Algorithmic Analysis Using Dataset-B

Figure 11 depicts the algorithmic analysis using dataset-B. The accuracy-based algorithmic analysis is provided in Fig. 11a. The accuracy of the methods, such as CSO + DRN, JOA + DRN, HBA + DRN, and implemented CJHBA + DRN, are 0.7926, 0.8410, 0.8426, and respectively. Similarly, the sensitivity analysis is shown in Fig. 11b. For 60% training data,

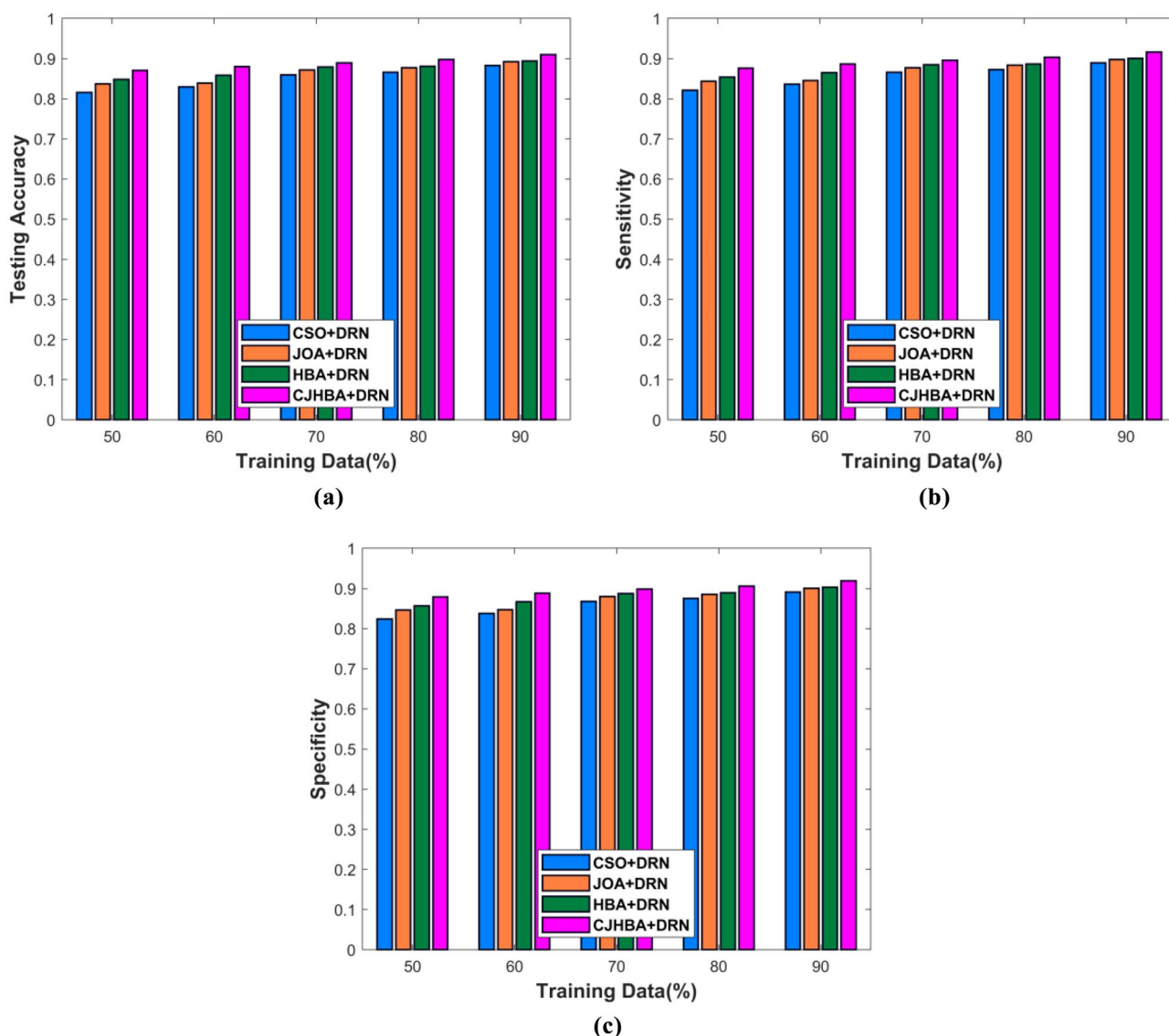


Fig. 10 Algorithmic analysis using dataset-A: **a** accuracy, **b** sensitivity, and **c** specificity

the sensitivity of the implemented CJHBA + DRN is 0.8608, and other methods, such as CSO + DRN, JOA + DRN, and HBA + DRN are 0.7919, 0.8026, and 0.8132, respectively. The specificity analysis is depicted in Fig. 11c. Likewise, for the same training percentage, the specificity of the implemented algorithm is 0.8695, whereas the CSO + DRN is 0.7846, JOA + DRN is 0.8097, and HBA + DRN is 0.8108. The performance is maximum for the highest training data percentage.

Comparative Discussion

Table 1 shows the comparative analysis of the brain tumor classification, and the values given in the table are attained at 90% training data. For considering the dataset-A, the testing accuracy of the implemented model is 0.9210, which is 3.88%,

3.49%, 2.53%, and 2.03% improved than other models, like transfer learning, BFC, DNN, and CNN, respectively. In the previously developed comparative methods, the DNN attained maximum sensitivity of 0.9110, but the proposed CJHBA-based DRN has improved 2.18% than the existing DNN. Similarly, the specificity of the implemented model is 0.9284, which is comparably higher than the previously developed techniques, like transfer learning, BFC, DNN, and CNN. The comparative discussion on dataset-B is discussed as follows: The maximum accuracy attained by the implemented technique is 0.9184, which is 10.90%, 8.06%, 5.66%, and 2.75% improved than the existing transfer learning, BFC, DNN, and CNN. The sensitivity of the implemented model is 0.9155, which is comparably higher than the previously developed techniques, like transfer learning, BFC, DNN, and CNN. Also, in the previously

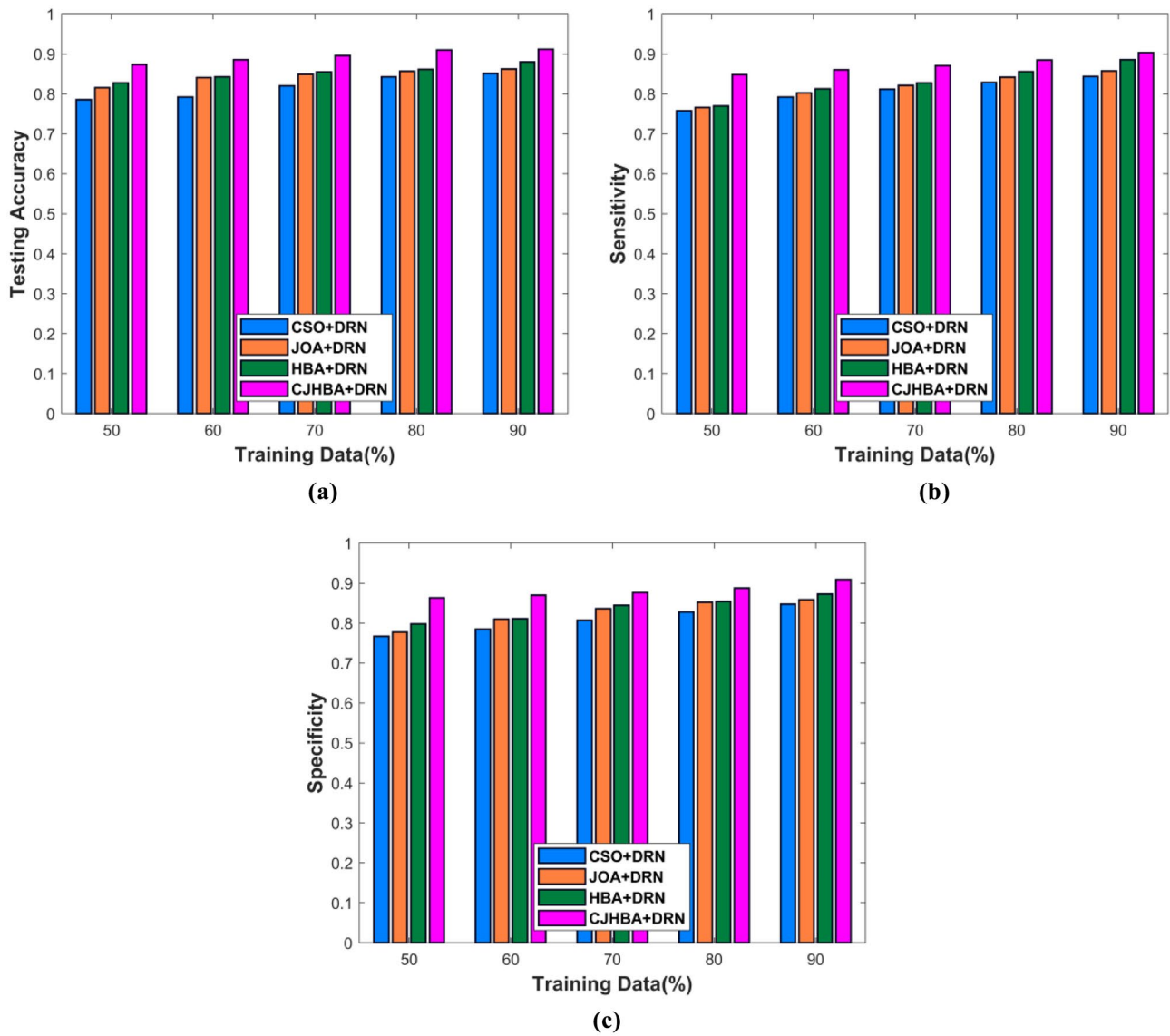


Fig. 11 Algorithmic analysis using dataset-B: **a** accuracy, **b** sensitivity, and **c** specificity

Table 1 Comparative analysis

Methods	Transfer learning	BFC	DNN	CNN	Implemented CJHBA-based DRN
Dataset-A					
Specificity	0.8883	0.8919	0.9007	0.9153	0.9284
Testing accuracy	0.8853	0.8889	0.8977	0.9023	0.9210
Sensitivity	0.8855	0.8988	0.9110	0.9075	0.9313
Dataset-B					
Specificity	0.8198	0.8494	0.8776	0.9031	0.9186
Testing accuracy	0.8183	0.8444	0.8664	0.8931	0.9184
Sensitivity	0.8184	0.8484	0.8684	0.8984	0.9155

The proposed method results are marked in bold font

Table 2 Algorithmic analysis

Methods	CSO + DRN	JOA + DRN	HBA + DRN	Implemented CJHBA + DRN
Dataset-A				
Specificity	0.8916	0.9004	0.9030	0.9189
Accuracy	0.8831	0.8919	0.8945	0.9104
Sensitivity	0.8893	0.8981	0.9007	0.9166
Dataset-B				
Specificity	0.8477	0.8586	0.8729	0.9089
Accuracy	0.8514	0.8626	0.8801	0.9114
Sensitivity	0.84363	0.85755	0.8857	0.9031

The proposed method results are marked in bold font

developed comparative methods, the CNN attained maximum specificity of 0.9186, but the proposed CJHBA-based DRN has improved 1.69% than the existing CNN.

The discussion of algorithmic analysis of the classification of tumors in the brain tumor is depicted in Table 2, and the values given in Table 2 are attained at 90% training data. From this table, it is proven that the implemented CJHBA + DRN has attained maximum accuracy, specificity, and sensitivity. While considering dataset-A, the implemented CJHBA + DRN attained maximum accuracy of 0.9104, sensitivity of 0.9166, and specificity of 0.9189. Similarly, the maximum specificity, accuracy, sensitivity, and specificity offered by considering the dataset-B are 0.9089, 0.9114, and 0.9031, respectively.

Conclusion

The brain tumor is the most dangerous abnormality, which is the unnatural and uncontrolled increase of brain cells. The exact and early diagnosis plays a main role in the treatment of patients. Hence, in this research, for segmenting and classifying the tumors in the brain, an efficient optimization-enabled deep learning approach is devised. In the devised technique, the MRI is initially pre-processed using a normalization scheme, and then, the segmentation is achieved using CHBA-based DeepMRSeg. After that, the CNN features are extracted for effectively classify the tumors in the brain. Then, the data augmentation is achieved and after data augmentation, the classification is performed using DRN. The DRN is trained using the proposed CJHBA, which is obtained by integrating the Jaya algorithm, HBA, and chronological concept. Thus, the proposed method effectively categorizes tumorous and non-tumorous patients. The efficiency of the implemented classification technique is evaluated using two publicly available datasets, like BRATS 2018 and Figshare, in which the maximum specificity, sensitivity, and accuracy are attained using the BRATS dataset with values 0.9284, 0.9313, and 0.9210, respectively. In the future, more features will be considered for enhancing

the performance of the developed model. Also, an effective method will be implemented for classifying the types of tumor and non-tumor tissues.

Acknowledgements I would like to express my very great appreciation to the co-authors of this manuscript for their valuable and constructive suggestions during the planning and development of this research work.

Author Contribution All authors have made substantial contributions to conception and design, revising the manuscript, and the final approval of the version to be published. Also, all authors agreed to be accountable for all aspects of the work in ensuring that questions related to the accuracy or integrity of any part of the work are appropriately investigated and resolved.

Data Availability The data underlying this article are available in BRATS 2018 dataset at <https://wiki.cancerimagingarchive.net/pages/viewpage.action?pageId=37224922> and Figshare dataset at https://figshare.com/articles/brain_tumor_dataset/1512427

Declarations

Ethical Approval Not applicable.

Informed Consent Not applicable.

Conflict of Interest The authors declare no competing interests.

References

1. David N. Louis, Arie Perry, Guido Reifenberger, Andreas von Deimling, Dominique Figarella-Branger, Webster K. Cavenee, Hiroko Ohgaki, Otmar D. Wiestler, Paul Kleihues, and David W. Ellison, The 2016 World Health Organization Classification of Tumors of the Central Nervous System: a summary, *Acta Neuropathol*, vol. 131, pp. 803–820, 2016.
2. Jaeyong Kang, Zahid Ullah, and Jeonghwan Gwak, MRI-Based Brain Tumor Classification Using Ensemble of Deep Features and Machine Learning Classifiers, *Sensors*, vol. 21, no. 6, 2021.
3. Gopal S. Tandel, Mainak Biswas, Omprakash G. Kakde, Ashish Tiwari, Harman S. Suri, Monica Turk, John R. Laird, Christopher K. Asare, Annabel A. Ankrah, N. N. Khanna, B. K. Madhusudhan, Luca Saba, and Jasjit S. Suri, A Review on a Deep Learning Perspective in Brain Cancer Classification, *Cancers*, vol. 11, no. 1, 2019.

4. Ahmad M. Sarhan, Brain Tumor Classification in Magnetic Resonance Images Using Deep Learning and Wavelet Transform, *Journal of Biomedical Science and Engineering*, vol. 13, no. 6, pp. 102–112, 2020.
5. Yurong Guan, Muhammad Aamir, Ziaur Rahman, Ammara Ali, Waheed Ahmed Abro, Zaheer Ahmed Dayo, Muhammad Shoaib Bhutta, and Zhihua Hu, A framework for efficient brain tumor classification using MRI images, *Mathematical Biosciences and Engineering*, vol. 18, no. 5, pp. 5790–5815, 2021.
6. Francisco Javier Díaz-Pernas, Mario Martínez-Zarzuela, Míriam Antón-Rodríguez, and David González-Ortega, A Deep Learning Approach for Brain Tumor Classification and Segmentation Using a Multiscale Convolutional Neural Network, *Healthcare*, vol. 9, no. 2, pp. 1–14, 2021.
7. Parnian Afshar, Konstantinos Plataniotis, and Arash Mohammadi, Capsule Networks for Brain Tumor Classification based on MRI Images and Course Tumor Boundaries, 2018.
8. Asmita Dixit and Aparajita Nanda, An improved whale optimization algorithm-based radial neural network for multi-grade brain tumor classification, *The Visual Computer*, 2021.
9. Jin Liu, Min Li, Jianxin Wang, Fangxiang Wu, Tianming Liu, and Yi Pan, A survey of MRI-based brain tumor segmentation methods, *Tsinghua Science and Technology*, vol. 19, no. 6, pp. 578–595, 2014.
10. G.Gokulkumari, Classification of Brain Tumor using Manta Ray Foraging Optimization-based DeepCNN Classifier, *Multimedia Research*, vol. 3, no. 4, pp. 32–42, 2020.
11. Xiaoqing Gu, Zongxuan Shen, Jing Xue, Yiqing Fan, and Tongguang Ni, Brain Tumor MR Image Classification Using Convolutional Dictionary Learning With Local Constraint, *Front Neuroscience*, 2021.
12. Avinash Gopal, Hybrid classifier: Brain Tumor Classification and Segmentation using Genetic-based Grey Wolf optimization, *Multimedia Research*, vol. 3, no. 2, pp. 1–10, 2020.
13. Zeynettin Akkus, Alfiia Galimzianova, Assaf Hoogi, Daniel L. Rubin, and Bradley J. Erickson, Deep Learning for Brain MRI Segmentation: State of the Art and Future Directions, *Journal of Digital Imaging*, vol. 30, pp. 449–459, 2017.
14. Isselmou Abd El Kader, Guizhi Xu, Zhang Shuai, Sani Saminu, Imran Javaid, and Isah Salim Ahmad, Differential Deep Convolutional Neural Network Model for Brain Tumor Classification, *Brain Sciences*, vol. 11, no. 3, 2021.
15. Heba Mohsen, El-Sayed A. El-Dahshan, El-Sayed M. El-Horbaty, and Abdel-Badeeh M. Salem, Classification using deep learning neural networks for brain tumors, *Future Computing and Informatics Journal*, vol. 3, no. 1, pp. 68–71, 2018.
16. Sérgio Pereira, Adriano Pinto, Victor Alves, and Carlos A. Silva, Brain Tumor Segmentation Using Convolutional Neural Networks in MRI Images, *IEEE Transactions on Medical Imaging*, vol. 35, no. 5, pp. 1240–1251, 2016.
17. Zhifang Zhan, Jian-Feng Cai, Di Guo, Yunsong Liu, Zhong Chen, and Xiaobo Qu, Fast Multiclass Dictionaries Learning With Geometrical Directions in MRI Reconstruction, *IEEE Transactions on Biomedical Engineering*, vol. 63, no. 9, pp. 1850–1861, 2016.
18. Jiang Wang, Yi Yang, Junhua Mao, Zhiheng Huang, Chang Huang, and Wei Xu, CNN-RNN: A Unified Framework for Multi-label Image Classification, In the proceeding of IEEE Conference on Computer Vision and Pattern Recognition (CVPR), 2016.
19. Jimit Doshi, Guray Erus, Mohamad Habes, and Christos Davatzikos, DeepMRSeg: A convolutional deep neural network for anatomy and abnormality segmentation on MR images, arXiv preprint [arXiv:1907.02110](https://arxiv.org/abs/1907.02110), 2019.
20. Hashim, F.A., Houssein, E.H., Hussain, K., Mabrouk, M.S. and Al-Atabany, W., Honey Badger Algorithm: New metaheuristic algorithm for solving optimization problems, *Mathematics and Computers in Simulation*, vol.192, pp.84–110, February 2022.
21. Yao, R., Wang, N., Liu, Z., Chen, P. and Sheng, X., Intrusion detection system in the advanced Metering infrastructure: a cross-layer feature-Fusion CNN-LSTM-Based approach, *Sensors*, vol.21, no.2, pp.626, January 2021.
22. BRATS 2018 database, taken from, https://figshare.com/articles/brain_tumor_dataset/1512427, accessed on February 2022.
23. Rao, R., Jaya: A simple and new optimization algorithm for solving constrained and unconstrained optimization problems, *International Journal of Industrial Engineering Computations*, vol.7, no.1, pp.19–34, 2016.
24. Javaria Amin, Muhammad Sharif, Nadia Gul, Mussarat Yasmin, and Shafqat Ali Shad, Brain tumor classification based on DWT fusion of MRI sequences using convolutional neural network, *Pattern Recognition Letters*, vol. 129, pp. 115–122, 2020.
25. Wadhah Ayadi, Imen Charfi, Wajdi Elhamzi, and Mohamed Atri, Brain tumor classification based on hybrid approach, *The Visual Computer*, vol. 38, pp. 107–117, 2022.
26. Swati, Z.N.K., Zhao, Q., Kabir, M., Ali, F., Ali, Z., Ahmed, S. and Lu, J., Brain tumor classification for MR images using transfer learning and fine-tuning, *Computerized Medical Imaging and Graphics*, vol.75, pp.34–46, 2019.
27. Figshare database, taken from, <https://wiki.cancerimagingarchive.net/pages/viewpage.action?pageId=37224922>, accessed on February 2022.
28. Chen, Z., Chen, Y., Wu, L., Cheng, S. and Lin, P., Deep residual network based fault detection and diagnosis of photovoltaic arrays using current-voltage curves and ambient conditions, *Energy Conversion and Management*, vol. 198, pp.111793, October 2019.
29. Raja, P.S., Brain tumor classification using a hybrid deep autoencoder with Bayesian fuzzy clustering-based segmentation approach, *Biocybernetics and Biomedical Engineering*, vol.40, no.1, pp.440–453, 2020.
30. Ghassemi, N., Shoeibi, A. and Rouhani, M., Deep neural network with generative adversarial networks pre-training for brain tumor classification based on MR images, *Biomedical Signal Processing and Control*, vol.57, pp.101678, 2020.
31. Mzoughi, H., Njeh, I., Wali, A., Slima, M.B., BenHamida, A., Mhiri, C. and Mahfoudhe, K.B., Deep multi-scale 3D convolutional neural network (CNN) for MRI gliomas brain tumor classification, *Journal of Digital Imaging*, vol.33, pp.903–915, 2020.
32. Ottorino Catani, Federico Fusini, Fabio Zanchini, Fabrizio Sergio, Giovanni Cautiero, Jorge Hugo Villafane, and Francesco Langella, Functional outcomes of percutaneous correction of hallux valgus in not symptomatic flatfoot: a case series study, *Acta Bio Medica: Atenei Parmensis*, vol. 91, no. 3, 2020.
33. Antonio Bonacaro, Ivan Rubbi, and Dave Sookhoo, The use of wearable devices in preventing hospital readmission and in improving the quality of life of chronic patients in the homecare setting: a narrative literature review, *Professioni Infermieristiche*, vol. 72, no. 2, pp. 143–151, 2019.
34. Maicol Carvello, Filippo Zanotti, Ivan Rubbi, Silvia Bacchetti, Giovanna Artioli, and Antonio Bonacaro, Peer-support: a coping strategy for nurses working at the Emergency Ambulance Service, *Acta Biomed for Health Professions*, vol. 90, no. 3, pp. 29–37, 2019.
35. Giovanni Parente, Tommaso Gargano, Giovanni Ruggeri, Michela Maffi, Simone D'Antonio, Elisa Sacchet, and Mario Lima, Anastomotic Stricture Definition After Esophageal Atresia Repair: Role of Endoscopic Stricture Index, *Journal of surgical research*, vol. 257, pp. 572–578, 2021.
36. Giovanni Parente, Tommaso Gargano, Stefania Pavia, Chiara Cordola, Marzia Vastano, Francesco Baccelli, Giulia Gallotta,

Laura Bruni, Adelaide Corvaglia, and Mario Lima, Pyelonephritis in pediatric uropathic patients: Differences from community-acquired ones and therapeutic protocol considerations. A 10-year single-center retrospective study, *Children*, vol. 8, no. 6, 2021.

Springer Nature or its licensor (e.g. a society or other partner) holds exclusive rights to this article under a publishing agreement with the author(s) or other rightsholder(s); author self-archiving of the accepted manuscript version of this article is solely governed by the terms of such publishing agreement and applicable law.

Publisher's Note Springer Nature remains neutral with regard to jurisdictional claims in published maps and institutional affiliations.